J. Fluid Mech. (2020), *vol.* 882, A28. © Cambridge University Press 2019
doi:10.1017/jfm.2019.824

Capillary surfaces in and around exotic cylinders with application to stability analysis

Fei Zhang[1,2] **and Xinping Zhou**[1,2,†]

[1]School of Mechanical Science and Engineering, Huazhong University of Science and Technology, Wuhan 430074, PR China

[2]Department of Mechanics, Huazhong University of Science and Technology, Wuhan 430074, PR China

(Received 4 December 2018; revised 8 October 2019; accepted 8 October 2019)

A capillary surface in or around exotic cylinders cannot locate itself, since the configurations of the exotic cylinders with a variable radius permit an entire continuum of equilibrium menisci, all of which have the same potential energy. The 'exotic' property indicates that all the menisci have the smallest eigenvalues $\lambda_1 = 0$ for the corresponding Sturm–Liouville problems without a volume constraint for stability analysis. Three types of exotic cylinders are addressed and the Sturm–Liouville problems with $\lambda = 0$ for stability analysis are solved numerically. Notably, the two-dimensional cases can be solved analytically. In the method of Slobozhanin & Alexander (*Phys. Fluids*, vol. 15, 2003, pp. 3532–3545), the stability of the meniscus is determined by comparing the boundary parameter χ_1 and the critical value χ_1^*, which is derived directly from the solution of the Sturm–Liouville problem with $\lambda = 0$. Results validate that the exotic cylinders have the boundary parameters $\chi_1 = \chi_1^*$. Motivated by this observation, a new way to determine the critical value χ_1^* under pressure disturbances for stability analysis is proposed without solving the Sturm–Liouville problem with $\lambda = 0$.

Key words: capillary flows

1. Introduction

Capillary phenomena in and around cylinders are ubiquitous throughout nature and in engineering processes, such as water transport in trees (Tyree 2003), capture of seeds by aquatic vegetation (Peruzzo *et al.* 2013) and measurement of contact angle (Decker *et al.* 1999). In each of these examples, the deformed surface (meniscus) in or around a vertical circular cylinder is determined uniquely by its contact angle and the cylinder radius (see e.g. White & Tallmadge (1965), Concus (1968), Huh & Scriven (1969)). However, some examples show that the configuration of a cylinder with a variable radius may permit two or more equilibrium menisci (Finn 1988). The uniqueness of the meniscus seems to be the exception rather than the rule (Concus & Finn 1991).

A striking observation that there exists an entire continuum of equilibrium menisci in an axisymmetric container for which the energy remains unchanged was first

† Email address for correspondence: xpzhou08@hust.edu.cn

made by Gulliver & Hildebrandt (1986), who studied the particular case of zero gravity and contact angle $\pi/2$. The general case was investigated by Finn (1988). A container with this remarkable property is called an exotic container. Most interestingly, the families of axisymmetric menisci in exotic containers turn out to be unstable (Finn 1988; Concus & Finn 1989; Wente 1999). This means that the menisci with a local minimum of energy are non-axisymmetric in the axisymmetric exotic containers, confirmed by numerical computations (Callahan, Concus & Finn 1991) and experiments (Concus, Finn & Weislogel 1992, 1999). Wente (2011) made the extension of the 'exotic' property to a capillary tube in an infinite bath, called an exotic capillary tube. Results showed that any axisymmetric equilibrium meniscus in an exotic tube is a minimiser of energy and hence has the same potential energy.

For stability analysis, disturbances of the menisci in the exotic container and the exotic tube are different (see Bostwick & Steen (2015) for a review). Only volume-preserving variations (called volume disturbances) of the interface are allowed in the case of an exotic container (because there is a volume constraint) and there is no volume constraint restricting the variations (called pressure disturbances) when one considers an exotic tube. For the exotic container, stability analysis predicts non-axisymmetric menisci (Finn 1988; Concus & Finn 1989; Wente 1999). These results are closely related to the non-axisymmetric instabilities of an axisymmetric surface subject to a volume constraint (Slobozhanin & Tyuptsov 1974). Based on the 'exotic' property, the second variation of energy in an exotic container is expected to be zero for axisymmetric perturbations (Wente 1999). Thus, non-axisymmetric perturbations are the most dangerous (i.e. corresponding to the smallest eigenvalue) in an exotic container, leading to three non-axisymmetric surface configurations (Concus *et al.* 1999). The non-axisymmetric instability can also be observed for an impaled drop and a liquid bridge when the Steiner limit is exceeded (Gillette & Dyson 1972; Slobozhanin, Alexander & Resnick 1997). However, the non-axisymmetric instability will not be observed in an exotic tube, because axisymmetric perturbations without a fixed volume constraint are more dangerous than non-axisymmetric ones (Myshkis *et al.* 1987; Slobozhanin & Alexander 2003). It seems obvious to conclude that any meniscus in an exotic tube has the smallest eigenvalue $\lambda_1 = 0$ for the corresponding Sturm–Liouville problem without a volume constraint, but questions remain about the mechanism underlying this observation. This may provide us with new insights into stability analysis.

In this work, we consider the meniscus formed in or around a vertical circular cylinder partially immersed in an infinite liquid under gravity. Then we unify the three configurations mentioned above (insets of figure 1) by the signed curvatures of the cylinder cross-sections and determine three corresponding exotic cylinders, where the exotic tube has been studied in depth by Wente (2011). The study is then extended to stability analysis for exotic cylinders. Using the method of Slobozhanin & Alexander (2003), the stability of the meniscus is determined by comparing the critical value χ_1^* and the boundary parameter χ_1 of the exotic cylinder, where the Sturm–Liouville problem $L_0\varphi_0 = 0$ is solved for χ_1^*. The spectral parameter power series (SPPS) method (Kravchenko & Porter 2010) is applied to the problems $L_0\varphi_0 = 0$ to obtain the contour lines of χ_1^* for two families of menisci. From the 'exotic' property, we expect that the meniscus in or around the exotic cylinder has the smallest eigenvalue $\lambda_1 = 0$ for the corresponding Sturm–Liouville problem without a volume constraint, leading to $\chi_1 = \chi_1^*$. This observation will be validated in our numerical experiments. Consideration of exotic cylinders in different ways will shed light on the physical and mathematical concepts underlying the 'exotic' property.

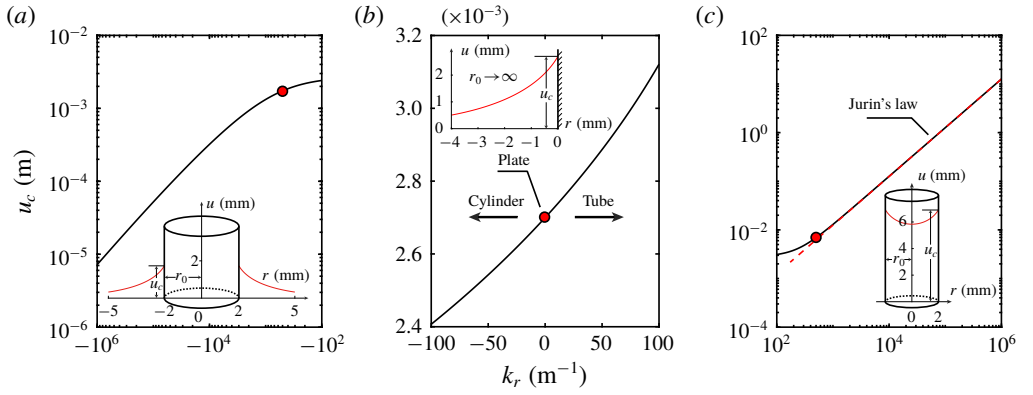

FIGURE 1. The influence of the signed curvature k_r of the cylinder cross-section on the contact line height u_c for $\theta = \pi/6$. The following values of parameters are used: $\sigma = 0.0715$ N m^{-1}, $g = 9.81$ m s^{-2} and $\rho = 1000$ kg m^{-3}. The insets in (*a–c*) show the configurations of $k_r = -500$, 0 and 500 m^{-1} (red dots), respectively. In the insets, the red lines denote the meniscus profiles with $u = 0$ located at the water line.

2. Determination of the exotic cylinders

2.1. *Axisymmetric menisci in and around a cylinder*

Consider a vertical circular cylinder partially immersed in an infinite water bath in a downward gravity field. The meniscus in or around the cylinder is determined uniquely by its contact angle θ and the cylinder radius r_0, as mentioned above. The configurations of the tube and cylinder can be unified by the signed curvature $k_r \equiv \pm 1/r_0$ of the cylinder cross-section, shown by $u_c(k_r)$ the height of the contact line as a function of k_r (figure 1). It is assumed that $k_r < 0$ (>0) if the cylinder cross-section is convex towards (away from) the liquid. Therefore, the case of $k_r = 0$ (i.e. $r_0 \to \infty$) corresponds to the configuration of a vertical flat plate (inset of figure 1*b*). For the vertical flat plate, the meniscus shape is described by (see e.g. Finn (2010), Bhatnagar & Finn (2016))

$$u = \frac{2}{\sqrt{\kappa}} \sin \frac{\psi}{2}, \tag{2.1a}$$

$$x - x_0 = \frac{1}{\sqrt{\kappa}} \left[2\cos\frac{\psi}{2} - 2\cos\frac{\psi_0}{2} + \ln\left(\frac{\tan\dfrac{\psi}{4}}{\tan\dfrac{\psi_0}{4}} \right) \right], \tag{2.1b}$$

where the subscript '0' indicates quantities evaluated at the plate, ψ is the inclination angle of the meniscus and $\kappa = \rho g/\sigma$ is the capillary constant, with density difference ρ (positive) between gas and liquid, gravitational acceleration g and surface tension σ of the interface. For $k_r \gg 0$, the height of the contact line can be given by Jurin's law (see the dashed red line in figure 1*c*):

$$u_c = 2k_r \cos\theta/\kappa, \tag{2.2}$$

where u_c and k_r are proportional. However, u_c and k_r for $k_r \ll 0$ (figure 1*a*) are not inversely proportional, confirmed by Hildebrand, Hildebrand & Tallmadge (1971).

These results are calculated numerically, based on the Young–Laplace equation in cylindrical coordinates (r, u) with the u-axis passing through the axis of the cylinder and $u = 0$ located at the undisturbed surface (Concus 1968):

$$\left[\frac{ru'}{(1+u'^2)^{1/2}}\right]' = \kappa r u, \tag{2.3}$$

where the prime refers to the derivative with respect to r. The boundary conditions are

$$u' = \tan(\pi/2 - \theta) \quad \text{at } r = 1/k_r, \tag{2.4a}$$
$$u' = 0 \quad \text{as } r \to -\infty, \quad \text{for } k_r < 0, \tag{2.4b}$$
$$u' = 0 \quad \text{at } r = 0, \quad \text{for } k_r > 0. \tag{2.4c}$$

This is a one-dimensional problem because the meniscus is axisymmetric. For the convenience of numerical calculation, equation (2.3) is expressed in a dimensionless parametric form by introducing the inclination angle ψ of the meniscus and using the dimensionless coordinate system (R, U) (with respect to the capillary length $1/\sqrt{\kappa}$). The dimensionless equations are (Huh & Scriven 1969)

$$\frac{\mathrm{d}R}{\mathrm{d}\psi} = \frac{R\cos\psi}{RU - \sin\psi}, \quad \frac{\mathrm{d}U}{\mathrm{d}\psi} = \frac{R\sin\psi}{RU - \sin\psi}, \tag{2.5a,b}$$

with the boundary conditions

$$R = 1/K_r \quad \text{at } \psi = \pi/2 - \theta, \tag{2.6a}$$
$$U \to 0 \quad \text{and} \quad R \to -\infty \quad \text{as } \psi \to 0, \quad \text{for } K_r < 0, \tag{2.6b}$$
$$R = 0 \quad \text{at } \psi = 0, \quad \text{for } K_r > 0, \tag{2.6c}$$

where K_r is the dimensionless curvature $k_r/\sqrt{\kappa}$.

The system of (2.5) with (2.6) can be solved numerically by the shooting method for solving a boundary-value problem by reducing it to the solution of an initial-value problem (Concus 1968; Rapacchietta & Neumann 1977). Because of the singularity of (2.5) at $\psi = 0$, the asymptotic solutions of the system as $\psi \to 0$ are taken as the initial conditions for the numerical integration of (2.5), given by (see Concus 1968; Huh & Scriven 1969)

$$U^* = \tan\psi^* \mathrm{K}_0(-R^*)/\mathrm{K}_1(-R^*), \quad \text{for } K_r < 0, \tag{2.7a}$$
$$U^* = \tan\psi^* \mathrm{I}_0(R^*)/\mathrm{I}_1(R^*), \quad \text{for } K_r > 0, \tag{2.7b}$$

where I and K are the modified Bessel functions of the first and second kinds, respectively. The appropriate value of ψ^* for (2.7) with a guessed value of R^* can be chosen as $\pm 0.01°$, where the upper (lower) sign is taken if $\theta < \pi/2$ $(> \pi/2)$. The Runge–Kutta method for integrating (2.5) and the secant method for adjusting R^* are used in the shooting method. Then the meniscus in or around a cylinder is determined.

2.2. *Shapes of the exotic cylinders*

Based on the above considerations, a mathematic model is formulated for determining the exotic cylinder with a given contact angle θ and an initial curvature $K_{in} = K_r$

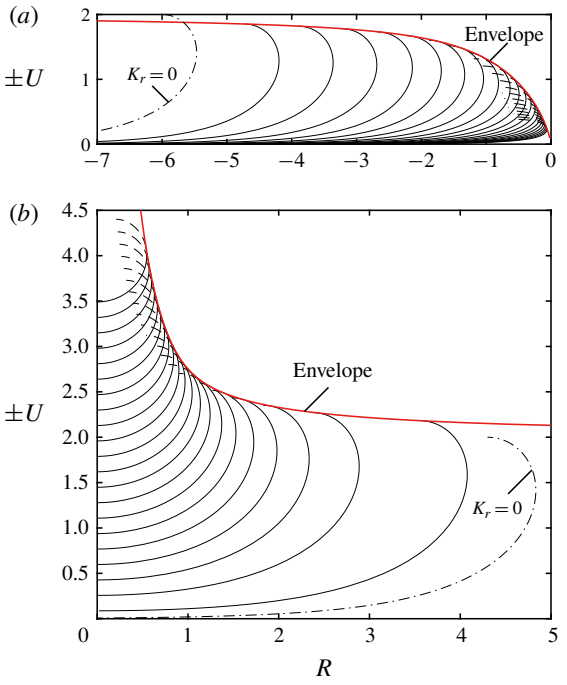

FIGURE 2. Two families of solution curves for $\psi \in [-\pi, \pi]$ (see also figure 2 in Huh & Scriven (1969) and figure 1 in Wente (2011)): (*a*) $K_r < 0$ and (*b*) $K_r > 0$. The thick red lines represent the envelopes of the solution curves, which divide the solution curves into two parts: $F(\psi, t) < 0$ for generating the shape of the exotic cylinder (solid lines) and $F(\psi, t) > 0$ (dashed lines). The dot-dashed lines represent the solution curves of $K_r = 0$ (i.e. the two-dimensional case), given by the dimensionless form of (2.1) with $\psi_0 = \pi$.

at $U = 0$. Wente (2011) has shown that the exotic tube ($K_r > 0$) can be determined by integrating the vector field $\langle \cos(\psi + \theta), \sin(\psi + \theta) \rangle$, constructed from the scalar field $\psi = \psi(R, U)$ with the Jacobian determinant $F(\psi, t)$ of $(R(\psi, t), U(\psi, t))$ being non-zero and remaining the same sign. Substituting (2.5) for the Jacobian determinant gives

$$F(\psi, t) = \frac{(-\dot{R} \sin \psi + \dot{U} \cos \psi) R}{RU - \sin \psi}, \tag{2.8}$$

where the overdot refers to the derivative with respect to the parameter t. Two families of solution curves of (2.5) with (2.6) are defined in parametric form by $(R(\psi, t), U(\psi, t))$ (see figure 2). Here the parameter t is chosen as R^* in (2.7) with ψ^* remaining unchanged. The region of $\psi(R, U)$ is bounded by the coordinate axes and the envelopes of the family curves in the R–U plane. The envelopes are found by solving $F(\psi, t) = 0$ numerically. In these cases, the numerical results show that the Jacobian determinant $F(\psi, t)$ is negative in the region (solid lines in figure 2) for generating the shape of the exotic cylinder while the Jacobian determinant in Wente (2011) is positive in the same region, because the parameter t is chosen as R^* in our cases while t is $U/2$ at $\psi = 0$ in Wente (2011).

Figure 2 shows two families of solution curves with $\psi \in [-\pi, \pi]$ for the axisymmetric menisci satisfying (2.5) with the conditions (2.6*b*) and (2.6*c*), respectively. In figure 2(*a*), the axisymmetric menisci with the condition (2.6*b*) extend outward to infinity and do not meet the axis of revolution. These menisci are called the axisymmetric fluid interfaces of unbounded extent by Huh & Scriven (1969). The envelope in figure 2(*a*) has a right endpoint $(R, U) \to (0, 0)$ and the height of the envelope is asymptotic to 2 as $R \to -\infty$. The height of the solution curve $K_r = 0$ equals 2 according to the dimensionless form of (2.1) with $\psi_0 = \pi$. Therefore, the envelope appears to transversally cross the curve $K_r = 0$ for the two-dimensional case in figure 2(*a*). In figure 2(*b*), the axisymmetric menisci with the condition (2.6*c*) are simply connected and are perpendicular to the axis of revolution at $R = 0$. The envelope in figure 2(*b*) is asymptotic to $RU = 2$ as $U \to +\infty$ and the height of the envelope decreases to 2 as $R \to +\infty$ and hence the envelope appears to miss the curve $K_r = 0$ in figure 2(*b*). Both the envelopes divide the solution curves into two parts: $F(\psi, t) < 0$ (solid lines) and $F(\psi, t) > 0$ (dashed lines). The first parts of the solution curves form the region of $\psi(R, U)$ for generating the shape of the exotic cylinder.

We make a natural extension of the cases of $K_r > 0$ studied by Wente (2011) to $K_r < 0$, where the menisci are formed around the cylinders. Then the shapes of the exotic cylinders (see figure 3) can be obtained by the above method of Wente (2011). The equations for determining the exotic cylinders are

$$\frac{\mathrm{d}X}{\mathrm{d}Y} = \cot(\psi + \theta), \tag{2.9a}$$

$$\psi = \psi(X, Y), \quad \text{for } F(\psi, R^*) < 0, \tag{2.9b}$$

with the initial conditions

$$X = \mp R_0, \quad \psi = 0 \quad \text{at } Y = 0, \tag{2.10a,b}$$

where the upper (lower) sign is taken if the cylinder cross-section is convex towards (away from) the liquid, $(X(Y), Y)$ denotes a point on the generatrix of the exotic cylinder and R_0 is the radius of the exotic cylinder at $U = 0$. As discussed above, the envelope in figure 2 bounds the region of $\psi(R, U)$ so that the exotic cylinder is also bounded by the corresponding envelope.

The system of (2.9) with (2.10) is solved numerically to generate the shapes of the exotic cylinders. The Runge–Kutta method is used to integrate (2.9*a*). Similar to the cases shown in figure 1, the interior, planar and exterior cases of the exotic cylinders shown in figure 3 are classified by the sign of the signed curvature $K_{in} = \pm 1/R_0$ (with the same sign rule as K_r) of the cross-section at the height $U = 0$, where the planar and exterior cases are new. Figure 3(*a*) shows three types of exotic cylinders with $\theta = \pi/4$ and $K_{in} = 1$, 0 and -1, and figure 3(*b*,*c*) compares the generatrices of exotic cylinders for different values of K_{in}.

For the interior cases ($K_{in} > 0$), as shown by Wente (2011), the exotic tube (thick red lines in figure 3) with $\theta \in (0, \pi/2)$ has a bottom tip at $Y = Y_m < 0$ and is asymptotic to $XY = 2\cos\theta$ as $Y \to +\infty$. For the case of $\theta = \pi/2$, the tube is asymptotic to $\lim XY = 0$ as $Y \to \pm\infty$ at both extremes.

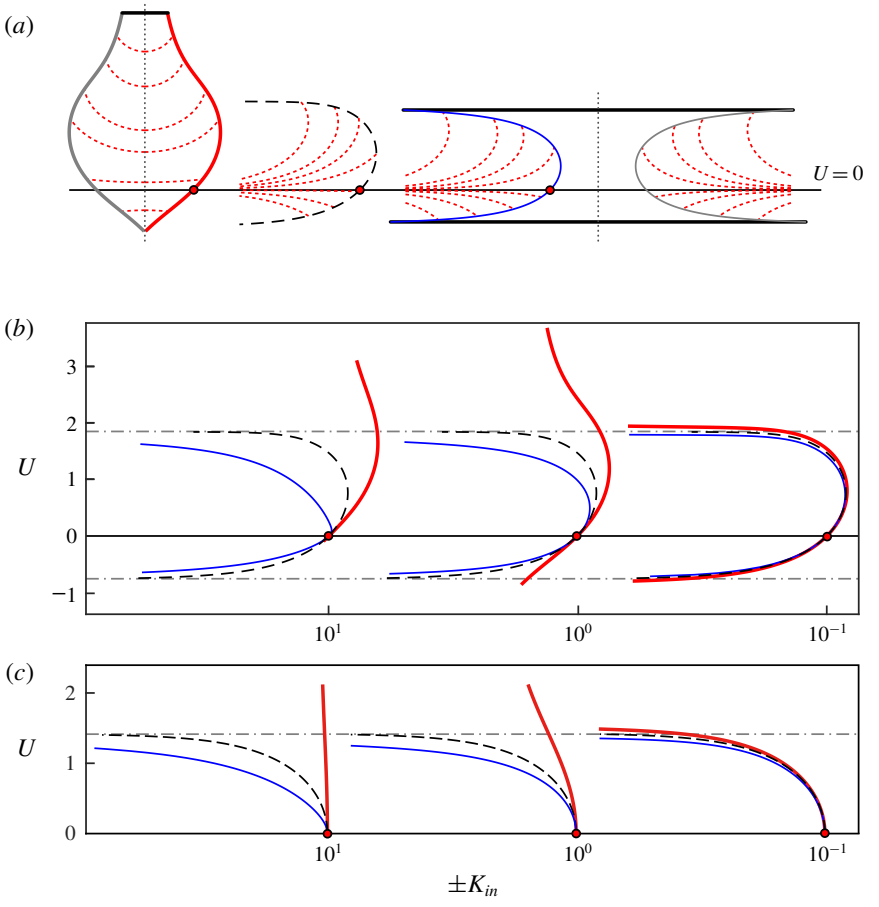

FIGURE 3. (*a*) Three types of exotic cylinders with $\theta = \pi/4$ and $K_{in} = 1$, 0 and -1 (from left to right), and (*b*,*c*) comparison between the shapes of the exotic cylinders with $K_{in} = 10^1$, 10^0 and 10^{-1} for (*b*) $\theta = \pi/4$ and (*c*) $\theta = \pi/2$. The thick solid red (thin blue) lines represent cases of $K_{in} > 0$ (<0), where the menisci are formed in (around) the exotic cylinders. In (*a*), the dotted lines represent the central axes and the dashed red lines represent the equilibrium menisci. The cases of $K_{in} = 0$ (dashed black lines) are determined by (2.12). The abscissa K_{in} indicates the reciprocal of R_0, where the central axis of the exotic cylinder is located at $R = 0$. The exotic cylinders with $K_{in} < 0$ are bounded by two horizontal (dot-dashed) lines $U = 2\cos(\theta/2)$ and $U = -2\sin(\theta/2)$.

For the exterior cases ($K_{in} < 0$), the exotic cylinder (thin blue lines in figure 3) is bounded by two horizontal lines $U = 2\cos(\theta/2)$ and $U = -2\sin(\theta/2)$, because the height of the meniscus is asymptotic to $2\sin(\psi/2)$ as $X \to -\infty$ with $\psi \to \pi - \theta$ ($-\theta$) for $Y > 0$ (<0) at the contact point. Thus, the height of the exotic cylinder with $K_{in} < 0$ is finite, given by $H < 2\sqrt{2}\sin[(2\theta + \pi)/4]$.

For the planar cases ($K_{in} = 0$), equation (2.9*b*) is given as $\psi = 2\sin^{-1}(Y/2)$. Then the exotic cylinder with $K_{in} = 0$ is described by

$$X(Y) = \int \cot[2\sin^{-1}(Y/2) + \theta]\,\mathrm{d}Y, \tag{2.11}$$

with $X(0)=X_0$. The indefinite integral (2.11) can be given explicitly as (see the dashed lines in figure 3)

$$X-X_0 = \sqrt{4-Y^2}-\cos\frac{\theta}{2}\ln\frac{\sqrt{4-Y^2}+2\cos\dfrac{\theta}{2}}{2\cos\dfrac{\theta}{2}(\sqrt{2-2\cos\theta}+Y)} - \sin\frac{\theta}{2}\ln\frac{\sqrt{4-Y^2}+2\sin\dfrac{\theta}{2}}{2\sin\dfrac{\theta}{2}(\sqrt{2+2\cos\theta}-Y)} - G(\theta), \tag{2.12}$$

where

$$G(\theta)=2-\cos\frac{\theta}{2}\ln\frac{1+\cos\dfrac{\theta}{2}}{\sin\theta}-\sin\frac{\theta}{2}\ln\frac{1+\sin\dfrac{\theta}{2}}{\sin\theta}. \tag{2.13}$$

In particular for $\theta=\pi/2$, the exotic wall (i.e. $K_{in}=0$) is described by

$$X-X_0=\sqrt{4-Y^2}-\sqrt{2}\ln\frac{\sqrt{4-Y^2}+\sqrt{2}}{\sqrt{4-2Y^2}}-G\left(\frac{\pi}{2}\right). \tag{2.14}$$

Additionally, compared to the case of $K_{in}=0$ (dashed black lines), the difference between the cases of $K_{in}=0$ and $K_{in}\neq 0$ becomes less with the decrease of $|K_{in}|$. Because of the symmetry of the solution curves in figure 2 with respect to the water line, the exotic cylinder with contact angle $\theta\in(\pi/2,\,\pi)$ is the inverse of that with contact angle $\pi-\theta\in(0,\,\pi/2)$ for all K_{in}. Thus, the exotic cylinder with contact angle $\theta=\pi/2$ is symmetric with respect to the R-axis. It is noted that the envelopes in figure 2 are tangent to all of the solution curves. Therefore, these envelopes can be regarded as the exotic cylinders with zero contact angle, but they do not intersect with the R-axis. In summary, we extend the exotic tube (Wente 2011) to the planar and exterior cases and the three cases are unified by the signed curvatures K_{in} of their cross-sections at $U=0$, as shown in figure 3.

3. Stability analysis

As discussed in § 1, because of the 'exotic' property, the menisci in and around exotic cylinders are expected to be stable, each of which corresponds to a critical state. Namely, each of the menisci has the smallest eigenvalue $\lambda_1=0$ for the corresponding Sturm–Liouville problem without a volume constraint. For the interior case, Wente (2011) used calibrations to prove that all menisci have minimum energy and therefore are stable. We have known that the profiles of the menisci for the exotic cylinders are the parts of the solution curves bounded by the envelopes in figure 2. Thus, a stability analysis for each of the menisci in figure 2 needs to be provided.

There are two methods to determine the stability of a meniscus: the direct computation method (see e.g. Myshkis *et al.* (1987), Slobozhanin *et al.* (1997), Pesci *et al.* (2015)) and the Poincaré–Maddocks method (Maddocks 1987; Lowry & Steen 1995). The former is used to solve the eigenvalue problem associated with the second variation of the system's total energy functional, while the latter predicts the stability changes inferred from turning points and bifurcations in the preferred diagram. In this work, stability is examined by the direct computation method proposed in Myshkis *et al.* (1987).

3.1. *Axisymmetric case*

We consider axisymmetric unperturbed menisci (in or around the exotic cylinders with $K_{in} \neq 0$) that can be described by the parametric dimensionless arclength variable S, which gives a parametric representation $R = R(S)$, $U = U(S)$ for the meniscus. The above parametric representation can be determined by the integration of (2.5) together with

$$\frac{\mathrm{d}S}{\mathrm{d}\psi} = \frac{R}{RU - \sin\psi}, \tag{3.1}$$

with the initial conditions (2.7) and $S(\psi^*) = 0$ with $\psi^* = 0.01^\circ$ (to avoid the singularity at $R = 0$). According to the approach of Myshkis *et al.* (1987), the perturbations are given by

$$\varphi = \varphi_0(S) + \sum_{n=1}^{\infty} [\varphi_n(S)\cos n\alpha + \phi_n(S)\sin n\alpha]. \tag{3.2}$$

It is known that axisymmetric perturbations without a fixed volume constraint are more dangerous than non-axisymmetric ones (Myshkis *et al.* 1987; Slobozhanin & Alexander 2003). Because the perturbations for the exotic cylinders are unconstrained, only the axisymmetric perturbation needs to be analysed in the study of stability, which leads to an eigenvalue problem (Myshkis *et al.* 1987)

$$L_0\varphi_0 \equiv -\varphi_0'' - \frac{R'}{R}\varphi_0' + a(S)\varphi_0 = \lambda\varphi_0, \quad \text{for } 0 \leqslant S \leqslant S_1, \tag{3.3}$$

$$\varphi_0'(S_1) + \chi_1\varphi_0(S_1) = 0, \tag{3.4}$$

with

$$a(S) \equiv \cos\psi - \tilde{K}_1^2 - \tilde{K}_2^2 \quad \text{and} \quad \chi_1 \equiv \frac{\tilde{K}_1(S_1)\cos\theta - \bar{K}}{\sin\theta}, \tag{3.5a,b}$$

where the prime refers to the derivative with respect to S and $\bar{K}$ is the dimensionless curvature of the generatrix of the exotic cylinder at the contact point ($\bar{K} < 0$ if the solid is convex to the liquid). Here, $S = S_1$ is the arc length of the profile where the meniscus meets the solid. The two dimensionless principal curvatures $\tilde{K}_1$ and $\tilde{K}_2$ of the fluid interface have the forms

$$\tilde{K}_1 = \frac{\mathrm{d}\psi}{\mathrm{d}S} = U - \frac{\sin\psi}{R} \quad \text{and} \quad \tilde{K}_2 = \frac{\sin\psi}{R}. \tag{3.6a,b}$$

It is noted that the boundary conditions at $S = 0$ are not given here, because the meniscus at $S = 0$ does not meet a solid. The boundary conditions at $S = 0$ need to be determined by the condition that the solution φ_0 is bounded at the symmetry axis for the case of $K_{in} > 0$ or at infinity for the case of $K_{in} < 0$.

The eigenvalues $\lambda_1, \lambda_2, \lambda_3, \ldots$ of the Sturm–Liouville problem (3.3)–(3.4) are real and can be ordered such that $\lambda_1 < \lambda_2 < \lambda_3 < \cdots < \lambda_n < \cdots \to \infty$. The smallest eigenvalue λ_1 of the above problem (3.3) with (3.4) corresponds to the minimum value of the second variation of the potential energy of the system. Thus the equilibrium is stable if $\lambda_1 > 0$, and is unstable if $\lambda_1 < 0$ (Alexander & Slobozhanin 2004).

For a fixed meniscus wetting a solid, the smallest eigenvalue λ_1 depends only on the boundary parameter χ_1, which is related to the contact angle and the dimensionless curvature of the generatrix of the solid (3.5*b*). The function $\lambda_1(\chi_1)$ is monotonically increasing (Myshkis *et al.* 1987). The eigenvalue λ_n varies monotonically with χ_1 for fixed mode n and this relation between λ_n and χ_1 is called modal monotonicity by Bostwick & Steen (2015). The value of the boundary parameter χ_1 letting $\lambda_1(\chi_1) = 0$ is termed the critical value χ_1^*.

Therefore, this problem can be further simplified by solving (3.3) with $\lambda = 0$ and then substituting the solution of the simplified problem $L_0\varphi_0 = 0$ into (3.4) to obtain the critical value $\chi_1^* = -\varphi_0'/\varphi_0$. For the problem $L_0\varphi_0 = 0$, the solution φ_0 also needs to satisfy the boundary conditions at $S = 0$ mentioned above. Based on the modal monotonicity, the equilibrium meniscus under pressure disturbances will be stable if $\chi_1 > \chi_1^*$, and unstable if $\chi_1 < \chi_1^*$ (Slobozhanin & Tyuptsov 1974). The existence of χ_1^* requires the meniscus $(0 \leqslant S \leqslant S_1)$ to be within the maximal stable profiles (i.e. $S_1 < S_1^*$), where the maximal stable profiles $(0 \leqslant S \leqslant S_1^*)$ denote the maximal possible profiles of stable equilibrium menisci. This means that a meniscus with $S_1 > S_1^*$ is always unstable under pressure disturbances in any container and at any wetting angle (Slobozhanin & Alexander 2003).

The Sturm–Liouville problem $L_0\varphi_0 = 0$ on a finite interval $[0, S_1]$ can be solved numerically by the SPPS method (Kravchenko & Porter 2010), which expresses the general solution of the Sturm–Liouville equation as a SPPS. In order to apply this method, the equation $L_0\varphi_0 = 0$ is transformed to the Sturm–Liouville form

$$(p\varphi_0')' = r\varphi_0, \tag{3.7}$$

where S_0 is an arbitrary point in $[0, S_1]$, $p = \exp(\int_{S_0}^{x} (R'/R)\mathrm{d}x)$ and $r = p(x)a(x)$.

We assume that the general solution is $\varphi_0 = c_1\varphi_1 + c_2\varphi_2$, where c_1 and c_2 are arbitrary constants. Based on the SPPS method, the two linearly independent regular solutions φ_1 and φ_2 can be calculated numerically by

$$\varphi_1 = \varphi_{00}\sum_{k=0}^{\infty}\tilde{X}^{(2k)} \quad \text{and} \quad \varphi_2 = \varphi_{00}\sum_{k=0}^{\infty}X^{(2k+1)}, \tag{3.8a,b}$$

with $\tilde{X}^{(n)}$ and $X^{(n)}$ being defined by the recursive relations

$$\tilde{X}^{(0)} \equiv 1, \quad X^{(0)} \equiv 1, \tag{3.9a,b}$$

$$\tilde{X}^{(n)}(S) = \begin{cases} \displaystyle\int_{S_0}^{S}\tilde{X}^{(n-1)}(x)\varphi_{00}^2(x)r(x)\,\mathrm{d}x, & n \text{ odd}, \\ \displaystyle\int_{S_0}^{S}\tilde{X}^{(n-1)}(x)\frac{1}{\varphi_{00}^2(x)p(x)}\mathrm{d}x, & n \text{ even}, \end{cases} \tag{3.9c}$$

$$X^{(n)}(S) = \begin{cases} \displaystyle\int_{S_0}^{S}X^{(n-1)}(x)\frac{1}{\varphi_{00}^2p(x)}\mathrm{d}x, & n \text{ odd}, \\ \displaystyle\int_{S_0}^{S}X^{(n-1)}(x)\varphi_{00}^2r(x)\,\mathrm{d}x, & n \text{ even}, \end{cases} \tag{3.9d}$$

where φ_{00} is a non-vanishing solution of $(p\varphi_0')' = 0$, typically chosen as the constant function $\varphi_{00} = 1$.

3.1.1. $K_{in} > 0$

The stability of an axisymmetric meniscus (simply connected) restricted by a constant-pressure constraint has been well studied by Slobozhanin & Alexander (2003). They have shown that the maximal stable profiles with $S \in [-R^*, S_1^*]$ can be determined from the first zero point of $\varphi_0(S)$, which is the solution of (3.7) with the condition that φ_0 is bounded at $S = -R^*$ (i.e. at the symmetry axis). To obtain the appropriate coefficients c_1 and c_2 for $\varphi_0 = c_1\varphi_1 + c_2\varphi_2$, the initial conditions need to be given at the point $S = 0$ corresponding to $\psi = \psi^*$, because the numerical calculation is conducted for $S \in [0, S_1]$. The initial conditions at $S = 0$ can be determined by the asymptotic solution of $L_0\varphi_0 = 0$ with $S \in [-R^*, 0]$ for small inclination angles.

For $S \in [-R^*, 0]$, $L_0\varphi_0 = 0$ simplifies to

$$\varphi_0'' + \frac{1}{S + R^*}\varphi_0' + \left(\frac{U^{*2}}{2} - 1\right)\varphi_0 = 0 \tag{3.10}$$

using the relations $R'/R \approx 1/(S + R^*)$ and $a \approx c = 1 - U^{*2}/2$ at small inclination angles, where U^* is given by (2.7). Equation (3.10) has the solution

$$\varphi_0 = \mathrm{I}_0((S + R^*)\sqrt{c}), \quad \text{for } U^{*2} < 2, \tag{3.11a}$$

$$\varphi_0 = 1, \quad \text{for } U^{*2} = 2, \tag{3.11b}$$

$$\varphi_0 = \mathrm{J}_0((S + R^*)\sqrt{-c}), \quad \text{for } U^{*2} > 2, \tag{3.11c}$$

which satisfies the condition that φ_0 is bounded at $S = -R^*$, where J is the Bessel function of the first kind. Differentiating (3.8) gives the expressions of φ_1' and φ_2':

$$\varphi_1' = \frac{1}{p}\sum_{k=1}^{\infty} \tilde{X}^{(2k-1)} \quad \text{and} \quad \varphi_2' = \frac{1}{p}\sum_{k=0}^{\infty} X^{(2k)}. \tag{3.12a,b}$$

If $S_0 = 0$ is chosen for (3.9), from the definitions of φ_1 and φ_2 we have $\varphi_1(0) = 1$, $\varphi_1'(0) = 0$, $\varphi_2(0) = 0$ and $\varphi_2'(0) = 1$. Then the coefficients c_1 and c_2 can be given by $c_1 = \varphi_0(0)$ and $c_2 = \varphi_0'(0)$, both of which are determined by (3.11). Last, the critical values $\chi_1^*(S)$ within the maximal stable profiles can be calculated by (3.4) together with (3.8) and (3.12), and further the stability of the meniscus is determined.

3.1.2. $K_{in} < 0$

Because the solution curves for $K_{in} < 0$ are infinitely long, the solution curves are divided into two parts: $S \in (-\infty, 0]$ and $S \in (0, S_1^*]$. The point $S = 0$ corresponds to the initial conditions (2.7*a*) for the integration of (2.5). The part $S \in (-\infty, 0]$ is solved asymptotically due to small inclination angles, and the part $S \in (0, S_1^*]$ is solved numerically by integrating (2.5) with (2.7*a*). Two linearly independent solutions φ_1 and φ_2 for $S \in (0, S_1^*]$ are determined by the mathematical model described in § 3.1. This model is suitable for both the axisymmetric cases $K_{in} > 0$ and $K_{in} < 0$.

Similar to the case of $K_{in} > 0$, the coefficients c_1 and c_2 for $\varphi_0 = c_1\varphi_1 + c_2\varphi_2$ also need to be determined from the conditions $\varphi_0(0)$ and $\varphi_0'(0)$, which are determined by the asymptotic solution for $S \in (-\infty, 0]$. The only difference is that the meniscus is formed around the cylinder and thus the condition for the solution of (3.7) is that φ_0 is bounded at $S \to -\infty$ (i.e. at $R \to -\infty$). For $S \in (-\infty, 0]$, the Sturm–Liouville problem $L_0\varphi_0 = 0$ simplifies to $\varphi_0'' + \varphi_0'/(S + R^*) - \varphi_0 = 0$ due to the small inclination angles. This equation has the solution

$$\varphi_0 = \mathrm{K}_0(-S - R^*), \tag{3.13}$$

which satisfies the condition that φ_0 is bounded at $S \to -\infty$. Then $c_1 = \varphi_0(0)$ and $c_2 = \varphi_0'(0)$ are determined by (3.13) and the appropriate solution $\varphi_0 = c_1\varphi_1 + c_2\varphi_2$ is obtained. Finally, the critical values $\chi_1^*(S)$ within the maximal stable profiles are calculated by $\chi_1^* = -\varphi_0'/\varphi_0$ and further the determination of stability is the same as before.

3.1.3. *Numerical results*

Using the SPPS method, the two linearly independent regular solutions φ_1 and φ_2 of the equation $L_0\varphi_0 = 0$ are determined. The appropriate solution is $\varphi_0 = c_1\varphi_1 + c_2\varphi_2$, where the coefficients c_1 and c_2 need to be determined. Then, the asymptotic solution of $L_0\varphi_0 = 0$ is determined by the condition that the appropriate solution φ_0 is bounded at the symmetry axis for the case of $K_{in} > 0$ or at infinity for the case of $K_{in} < 0$, and the initial conditions at $S = 0$ (i.e. $\varphi_0(0)$ and $\varphi_0'(0)$) can be given by the asymptotic solution. The coefficients c_1 and c_2 are determined from the initial conditions $\varphi_0(0)$ and $\varphi_0'(0)$. Finally, the appropriate solution $\varphi_0 = c_1\varphi_1 + c_2\varphi_2$ is determined.

After determining the appropriate solutions φ_0 of (3.7) for different values of R^*, the critical values χ_1^* within the maximal stable profiles can be easily determined, as shown in figure 4. In figure 4(*a*), we reproduce the diagram of stability to pressure disturbances by fixing the left-hand tip points of the meniscus profiles to the origin (see also figure 3 in Slobozhanin & Alexander (2003)). In these cases, the value of meniscus height at the axis of symmetry is approximately equal to U^* because of the small value $\psi^* = 0.01°$.

To clearly illustrate the stability diagrams, two families of solution curves (figure 2) are contoured with a set of values of χ_1^*, as shown in figure 4(*b*,*c*). Figures 4(*b*) and 4(*c*) give the critical values χ_1^* for the two families of solution curves in figures 2(*b*) and 2(*a*), respectively. As mentioned above, the equilibrium meniscus under pressure disturbances will be stable if $\chi_1 > \chi_1^*$, and unstable if $\chi_1 < \chi_1^*$, where χ_1 is the boundary parameter related to the contact angle and the dimensionless curvature of the generatrix of the solid (3.5*b*). Any meniscus for the exotic cylinders has an end point (R, U) and the critical value χ_1^* at (R, U) in figure 4 is applied for the stability analysis. The contour lines $\chi_1^* = \infty$ divide the solution curves (figure 2) into two parts, and only the lower curves corresponding to the maximal stable profiles (thick black lines in figure 4) are plotted.

We found that there are two regions $-1 < \chi_1^* < 0$ and $\chi_1^* > 0$ separated by the contour line $\chi_1^* = 0$ in figure 4(*b*). The line $\chi_1^* = 0$ only intersects with the solution curves with $U^{*2} \leqslant 2$ and there is only one intersection point for each of the solution curves. In the region $-1 < \chi_1^* < 0$, the contour line intersects with the abscissa at $(R_c, 0)$ which satisfies the relation (Slobozhanin & Alexander 2003)

$$\chi_1^* = -\mathrm{I}_1(R_c)/\mathrm{I}_0(R_c). \tag{3.14}$$

We can see that $\chi_1^* \to -1$ as $R_c \to \infty$. In the region $\chi_1^* > 0$, the contour lines will intersect with all solution curves, and there is only one intersection point for each of the solution curves. In particular, the line $\chi_1^* = \infty$ is the boundary line of the maximal stable profiles. In figure 4(*c*), the stability diagram is also divided into two regions $\chi_1^* > -1$ and $\chi_1^* < -1$ by the contour line $\chi_1^* = -1$. In the region $\chi_1^* < -1$, the contour line intersects with the abscissa at $(\bar{R}_c, 0)$ which satisfies the relation

$$\chi_1^* = -\mathrm{K}_1(-\bar{R}_c)/\mathrm{K}_0(-\bar{R}_c). \tag{3.15}$$

Most interestingly, the numerical results show that the contour lines $\chi_1^* = \infty$ (figure 4*b*,*c*) are in good agreement with the envelopes of solution curves (figure 2). We will discuss these results in § 3.3.

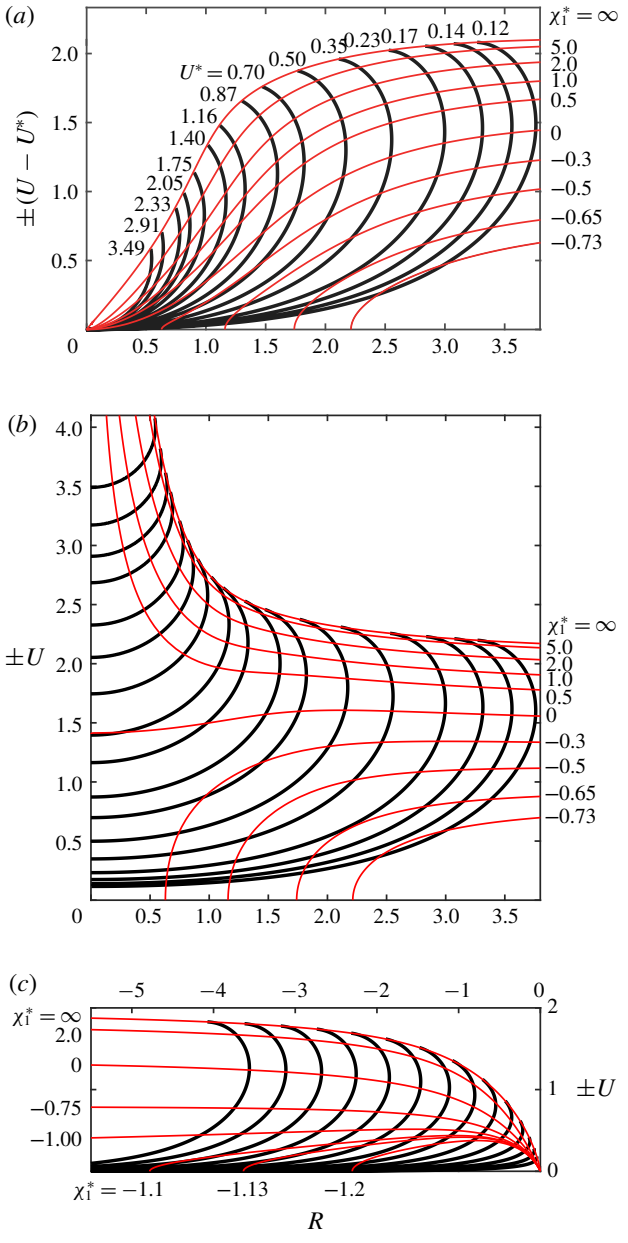

FIGURE 4. Stability to pressure disturbances for axisymmetric menisci: (*a*) the solution curves fixed at the origin for $K_{in} > 0$ (see also figure 3 in Slobozhanin & Alexander (2003)) and (*b*,*c*) the solution curves with $U = 0$ located at the water line for (*b*) $K_{in} > 0$ and (*c*) $K_{in} < 0$. Panel (*b*) is essentially the same as panel (*a*) except for the different choices of the ordinates. The thick black lines denote the maximal stable profiles to pressure disturbances and the thin red lines denote the contour lines of χ_1^*. The end point of the maximal stable profile corresponds to $\chi_1^* = \infty$. In these calculations, the order k for (3.8) is given as $k = 12$.

3.2. *Two-dimensional case*

Similar to the approach taken for the stability for $K_{in} \neq 0$, the stability of the two-dimensional meniscus ($K_{in} = 0$) can be determined by solving the problem

$$L_0\varphi_0 \equiv -\varphi_0'' + a(S)\varphi_0 = 0, \quad \text{for } 0 \leqslant S \leqslant S_1, \tag{3.16}$$

where $a(S) = 3\cos\psi - 2$ is derived from (3.5*a*). We assume $S = 0$ at a small inclination angle $\psi_0 = 0.01°$. Then the parametric representation $S(\psi)$ is given by

$$S(\psi) = \int_{\psi_0}^{\psi} \frac{1}{U(\psi)} \mathrm{d}\psi = \ln\left(\tan\frac{\psi}{4} \Big/ \tan\frac{\psi_0}{4}\right). \tag{3.17}$$

The inverse of (3.17) is

$$\psi(S) = 4\tan^{-1}(\exp(S + S_0)), \tag{3.18}$$

where $S_0 = \ln(\tan(\psi_0/4))$. Then

$$a(S) = \frac{\exp(4S + 4S_0) - 22\exp(2S + 2S_0) + 1}{\exp(4S + 4S_0) + 2\exp(2S + 2S_0) + 1}. \tag{3.19}$$

To apply the SPPS method to this problem, equation (3.16) is transformed to the form of $(p\varphi_0')' = r\varphi_0$, where $p = 1$ and $r = a(S)$. Then two independent solutions φ_1 and φ_2 are given by (3.8). The boundary condition at $S = 0$ can be obtained from the solution of $\varphi_0'' = a\varphi_0$ for $S \leqslant 0$ (corresponding to $\psi \in (0, \psi_0]$), where $a \approx 1$ at small inclination angles or $a = 1$ for flat menisci. The solution that satisfies that φ_0 is bounded as $S \to -\infty$ is $\exp(S)$. Thus the conditions at $S = 0$ are $\varphi_0(0) = 1$ and $\varphi_0'(0) = 1$, and hence $\varphi_0 = \varphi_1 + \varphi_2$ with $S_0 = 0$. Then the critical values χ_1^* are determined.

Figure 5(*a*) shows the numerical solution φ_0 calculated by the SPPS method, where the boundary conditions at $S = 0$ are given by the solution $\varphi_0 = \exp(S)$ (see the left-hand inset). The first zero point of φ_0 (the yellow point) corresponds to the maximal stable profile, as shown in the right-hand inset. The numerical result indicates that the end point of the maximal stable profile is the point with $U \approx 2$ ($|U - 2| = 4.3 \times 10^{-10}$), corresponding to an inclination angle $\psi = \pi$, where the order of the SPPS method is $k = 12$. Similar to the axisymmetric case, the stability can be determined by the critical values χ_1^*, as shown in figure 5(*b*). The critical values χ_1^* can be uniquely determined by the inclination angle ψ. It is known that this meniscus is invariant under translation in R. Thus the contour lines for χ_1^* are the horizontal straight lines. Specifically, the lines $U = \pm 2$ are the contour lines $\chi_1^* = \infty$, and also the envelopes of the two-dimensional menisci.

3.3. *Stability analysis of exotic cylinders and 'exotic' property*

The profiles of the menisci in or around the exotic cylinder are the parts of the solution curves in figure 4(*b*,*c*), each of which meets the exotic cylinder at a prescribed contact angle θ. Then, the stabilities of the menisci are determined by comparing the boundary parameters χ_1 of the exotic cylinder and the critical values χ_1^*. The meniscus under pressure disturbances will be stable if $\chi_1 > \chi_1^*$, and unstable if $\chi_1 < \chi_1^*$.

For the exotic cylinders with $K_{in} > 0$, Wente (2011) has shown that any (equilibrium) meniscus in the exotic cylinder is a minimiser of energy. This means that the second

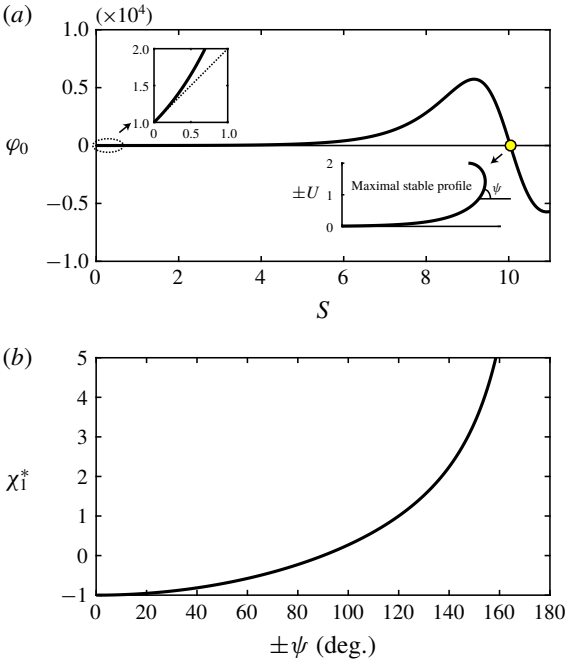

FIGURE 5. (*a*) Numerical result of (3.16) calculated by the SPPS method and (*b*) relation between χ_1^* and ψ.

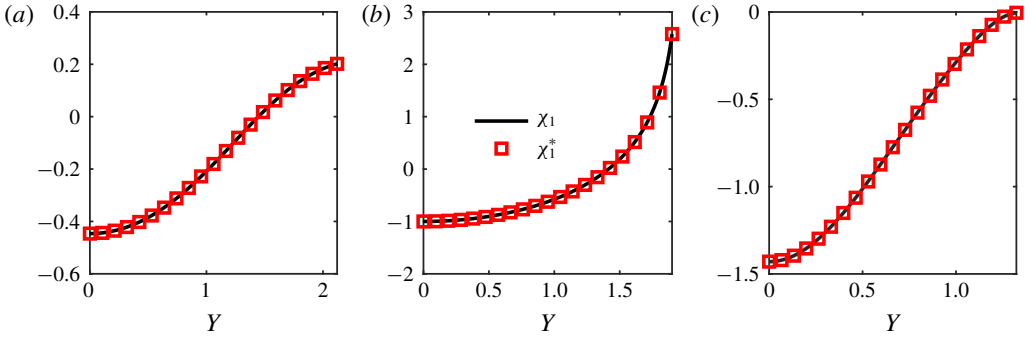

FIGURE 6. Comparison between the critical values χ_1^* and the boundary parameters of χ_1 of the exotic cylinders with contact angle $\theta = \pi/2$ and parameters $K_{in} = 1$ (*a*), 0 (*b*) and -1 (*c*). The abscissa Y denotes the height of the exotic cylinder.

variation of energy is zero to pressure disturbances. This case can be extended to the cases of $K_{in} < 0$ and $K_{in} = 0$ (see appendix A). Therefore, the boundary parameter χ_1 of the exotic cylinder is expected to be equal to the critical value χ_1^*. This observation is validated in our numerical experiments. Figure 6 shows that, as expected, there is a good agreement between the critical values χ_1^* and the boundary parameters χ_1 of the exotic cylinders for $K_{in} = 1$, 0 and -1. This means that the smallest eigenvalue of the Sturm–Liouville problem for the meniscus in or around the exotic cylinders is equal to zero under pressure disturbances. Although these results may seem not surprising at first, they provide another way to determine stability, because the critical values χ_1^*

are equal to the boundary parameters χ_1 of the exotic cylinders. Namely, the critical values χ_1^* can be determined by calculating the boundary parameters χ_1 of the exotic cylinders by (3.5*b*), not by solving the Sturm–Liouville problem $L_0\varphi_0 = 0$.

3.3.1. *Two-dimensional case*

For $K_{in} = 0$, substituting (2.11) into $\bar{K} = -X''/(1 + X'^2)^{3/2}$ with $Y = 2\sin(\psi/2)$ gives

$$\bar{K} = \frac{\sin(\psi + \theta)}{\cos\dfrac{\psi}{2}}, \tag{3.20}$$

where $\bar{K}$ is the signed curvature of the exotic cylinder. Substituting (3.20) into (3.5*b*) with $\tilde{K}_1 = 2\sin(\psi/2)$ and $\chi_1^* = \chi_1$, we have

$$\chi_1^* = -\frac{\cos\psi}{\cos\dfrac{\psi}{2}}. \tag{3.21}$$

To verify this equation, substituting (3.21) into (3.4) gives

$$\varphi_0' = \frac{\cos\psi}{\cos\dfrac{\psi}{2}}\varphi_0. \tag{3.22}$$

Then the differential equation (3.22) is solved using the 'dsolve' program in MATLAB for the analytical solution

$$\varphi_0 = \frac{\exp(S)[\exp(2S + 2S_0) - 1]}{[\exp(2S + 2S_0) + 1]^2}, \tag{3.23}$$

which satisfies (3.16). Thus (3.21) is verified and provides an analytical expression for the critical value χ_1^* for the two-dimensional meniscus.

Interestingly, the property of the exotic cylinder is related to the floating phenomenon. It is known that the meridional curvature of the exotic cylinder with $K_{in} = 0$ is given by (3.20). This expression can also be deduced from the relation between the variations δH and δU (see appendix B in Zhang, Zhou & Zhu (2018)):

$$\left[\cos\frac{\psi}{2} - \frac{1}{\bar{K}}\sin(\psi + \theta)\right]\delta U = \cos\frac{\psi}{2}\delta H, \tag{3.24}$$

where all the quantities are dimensionless, $\bar{K}$ denotes the curvature of solid at the contact point, ψ denotes the inclination angle of the meniscus at the contact point and δU and δH denote the variations of the contact point height and the vertical displacement of floating body, respectively. This equation provides quantitative relations between the infinitesimal vertical displacement δH of a two-dimensional floating body and the change δU of the contact point height. This means that in response to an infinitesimal vertical displacement δH of the floating body, the equilibrium meniscus will adjust itself, leading to a change of the contact point height δU. For the exotic cylinders with $K_{in} = 0$, the coefficient $[\cos(\psi/2) - (1/\bar{K})\sin(\psi + \theta)]$ for δU will be zero, because δU can be arbitrary when the exotic cylinder is fixed ($\delta H = 0$). Then (3.20) is derived. This finding seems

to provide a useful way to calculate the curvature of the exotic cylinder and then to determine stability without solving the Sturm–Liouville problem $L_0\varphi_0 = 0$.

Additionally, it is noted that the envelopes can be regarded as exotic cylinders with $\theta = 0$, because the envelopes are tangent to all menisci. Seen from (3.5*b*), we have $\chi_1 = \infty$ for the exotic cylinders with $\theta = 0$. Therefore, it is not surprising that the envelopes are in good agreement with the contour lines $\chi_1^* = \infty$ in figure 4. Therefore, the maximal stable profiles can be determined by solving $F(\psi, t) = 0$.

3.3.2. *Axisymmetric case*

The exotic cylinder with $K_{in} < 0$ can also be regarded as a special floating body with a fixed position in which the contact point is allowed to move continuously on the solid. This idea also applies to the case of $K_{in} > 0$. Suppose that $U(R, \psi)$ determines the families of curves in figure 2. Then the signed curvature of the generatrix of the exotic cylinder at the contact point satisfies the relation

$$\bar{K} \equiv \left.\frac{\mathrm{d}\bar{\psi}}{\mathrm{d}\bar{S}}\right|_S = \frac{\sin\bar{\psi}}{\left.\dfrac{\mathrm{d}U}{\mathrm{d}\psi}\right|_S}, \tag{3.25}$$

where the inclination angle of the solid satisfies $\bar{\psi} = \psi + \theta$ (the 'exotic' property), $\bar{S}$ denotes the arc length of the solid and the subscript 'S' denotes that the total derivative is constrained to the solid. Then we obtain

$$\left.\frac{\mathrm{d}U}{\mathrm{d}\psi}\right|_S = \frac{\partial U}{\partial\psi} + \frac{\partial U}{\partial R}\left.\frac{\mathrm{d}R}{\mathrm{d}U}\right|_S \left.\frac{\mathrm{d}U}{\mathrm{d}\psi}\right|_S, \tag{3.26}$$

where $\mathrm{d}R/\mathrm{d}U|_S = \cot\bar{\psi}$. This gives

$$\bar{K} = \frac{\sin\bar{\psi}}{\dfrac{\partial U}{\partial\psi}}\left(1 - \cot\bar{\psi}\frac{\partial U}{\partial R}\right). \tag{3.27}$$

It is noted that another expression for $\bar{K}$ has been proposed in Huh & Mason (1974) using the relation between δH and δU, similar to (3.24). For the curvature of the meniscus at the contact point, a similar derivation gives

$$\tilde{K}_1 = \frac{\sin\psi}{\dfrac{\partial U}{\partial\psi}}\left(1 - \cot\psi\frac{\partial U}{\partial R}\right). \tag{3.28}$$

The curvature of the meniscus is also represented by (3.6*a*), and therefore the relation between $\partial U/\partial\psi$ and $\partial U/\partial R$ is

$$\frac{\partial U}{\partial\psi} = \frac{R\sin\psi}{RU - \sin\psi}\left(1 - \cot\psi\frac{\partial U}{\partial R}\right). \tag{3.29}$$

Then substituting (3.27), (3.28) and (3.29) into (3.5*b*) gives the boundary parameter of the exotic cylinder:

$$\chi_1 = \chi_1^* = -\frac{(RU - \sin\psi)\left(\cos\psi + \sin\psi\dfrac{\partial U}{\partial R}\right)}{R\left(\sin\psi - \cos\psi\dfrac{\partial U}{\partial R}\right)}, \tag{3.30}$$

which is independent of θ. The critical value χ_1^* can be determined as long as $\partial U/\partial R$ is determined. The partial derivative $\partial U/\partial R$ can be determined by integrating (2.5) together with

$$\frac{\mathrm{d}(\partial U/\partial R)}{\mathrm{d}\psi} = \frac{\partial(\partial U/\partial R)}{\partial \psi} + \frac{\partial(\partial U/\partial R)}{\partial R}\frac{\mathrm{d}R}{\mathrm{d}\psi}. \tag{3.31}$$

Suppose that U is a new variable. We have

$$\left.\frac{\mathrm{d}(\mathrm{d}U/\mathrm{d}\psi)}{\mathrm{d}R}\right|_{\psi=\text{const.}} = \frac{\partial(\mathrm{d}U/\mathrm{d}\psi)}{\partial R} + \frac{\partial(\mathrm{d}U/\mathrm{d}\psi)}{\partial U}\frac{\partial U}{\partial R}, \tag{3.32}$$

where $\partial(\mathrm{d}U/\mathrm{d}\psi)/\partial R$ and $\partial(\mathrm{d}U/\mathrm{d}\psi)/\partial U$ are the partial derivatives of (2.5). On the other hand, (3.32) can also be written as

$$\begin{aligned}\left.\frac{\mathrm{d}(\mathrm{d}U/\mathrm{d}\psi)}{\mathrm{d}R}\right|_{\psi=\text{const.}} = {} & \frac{\partial(\partial U/\partial R)}{\partial R}\frac{\mathrm{d}R}{\mathrm{d}\psi} + \frac{\partial(\partial U/\partial \psi)}{\partial R} \\ & + \left[\frac{\partial(\mathrm{d}R/\mathrm{d}\psi)}{\partial R} + \frac{\partial(\mathrm{d}R/\mathrm{d}\psi)}{\partial U}\frac{\partial U}{\partial R}\right]\frac{\partial U}{\partial R},\end{aligned} \tag{3.33}$$

where $\partial(\mathrm{d}R/\mathrm{d}\psi)/\partial R$ and $\partial(\mathrm{d}R/\mathrm{d}\psi)/\partial U$ are the partial derivatives of (2.5). Comparing (3.31), (3.32) and (3.33), we find

$$\begin{aligned}\frac{\mathrm{d}(\partial U/\partial R)}{\mathrm{d}\psi} = {} & \frac{\partial(\mathrm{d}U/\mathrm{d}\psi)}{\partial R} + \frac{\partial(\mathrm{d}U/\mathrm{d}\psi)}{\partial U}\frac{\partial U}{\partial R} \\ & - \left[\frac{\partial(\mathrm{d}R/\mathrm{d}\psi)}{\partial R} + \frac{\partial(\mathrm{d}R/\mathrm{d}\psi)}{\partial U}\frac{\partial U}{\partial R}\right]\frac{\partial U}{\partial R}.\end{aligned} \tag{3.34}$$

By integrating (3.34) together with (2.5) and then substituting the value of $\partial U/\partial R$ for (3.30), the critical value χ_1^* is obtained, where the initial condition for $\partial U/\partial R$ is given by the partial derivatives of (2.7). Figure 7 shows a good agreement between the contour lines $\chi_1^* = 0$ calculated by solving the Sturm–Liouville problem $L_0\varphi_0 = 0$ and by (3.30). Thus, by utilising the property of the exotic cylinder we find a convenient alternative for calculating the critical value χ_1^* and then determining the stability of the axisymmetric meniscus under pressure disturbances.

For (3.30), we make the following simple observations. (i) For $\chi_1^* \to \infty$ (i.e. $\sin\psi - \cos\psi(\partial U/\partial R) = 0$), this equation determines the maximal stable profiles (see figure 4), and also the envelopes of menisci (see figure 2), and therefore the equation is equivalent to $F(\psi, t) = 0$ when t is chosen as R with ψ held constant. (ii) Equation (3.30) can be written in a generalised form:

$$\chi_1 = \chi_1^* = -\frac{\cos\psi + \sin\psi\dfrac{\partial U}{\partial R}}{\dfrac{\partial U}{\partial \psi}}, \tag{3.35}$$

which can degenerate to (3.21) when $U = 2\sin(\psi/2)$ for the two-dimensional case.

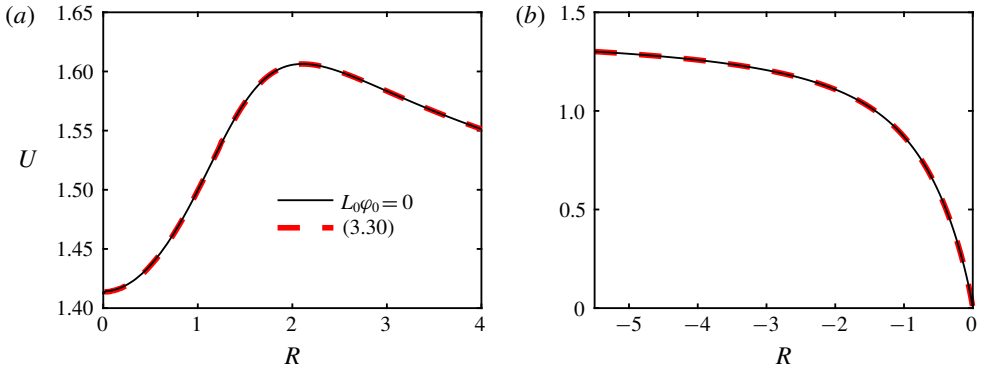

FIGURE 7. Comparison between the contour lines $\chi_1^* = 0$ by solving the Sturm–Liouville problem $L_0\varphi_0 = 0$ and by (3.30) for (*a*) $K_{in} > 0$ and (*b*) $K_{in} < 0$.

4. Conclusions

In this paper, we have investigated three types of exotic cylinders classified by the signed curvatures K_{in} of their cross-sections at $U = 0$, where the interior case $K_{in} > 0$ has been studied in depth by Wente (2011). Three types of exotic cylinders are determined by integrating the vector field $\langle \cos(\psi + \theta), \sin(\psi + \theta) \rangle$. Different from the interior case $K_{in} > 0$, the exotic cylinder for the exterior case $K_{in} < 0$ is bounded by two horizontal lines $U = 2\cos(\theta/2)$ and $U = -2\sin(\theta/2)$. Specifically, the analytical expression (2.12) for the planar case $K_{in} = 0$ is obtained. Interestingly, the envelope of the menisci can be regarded as a special exotic cylinder with $\theta = 0$, because the envelope is tangent to all menisci.

The study is then extended to examine the stabilities of menisci in and around the exotic cylinders. In the method of Slobozhanin & Alexander (2003), the stability of the meniscus to pressure disturbances is determined by comparing the critical value χ_1^* and the boundary parameter χ_1, where the Sturm–Liouville problem $L_0\varphi_0 = 0$ is solved for χ_1^*. The meniscus under pressure disturbances will be stable if $\chi_1 > \chi_1^*$, and unstable if $\chi_1 < \chi_1^*$. The SPPS method is applied to the problems $L_0\varphi_0 = 0$ to obtain the contour lines of χ_1^* for two families of menisci, as shown in figure 4. For the two-dimensional case, χ_1^* only depends on the inclination angle of the meniscus (see figure 5*b*). Based on the 'exotic' property (Wente 2011), one would expect that each of the menisci has the smallest eigenvalue $\lambda_1 = 0$ for the corresponding Sturm–Liouville problem without a volume constraint. Thus, the boundary parameters χ_1 of the exotic cylinders are expected to be equal to χ_1^*, validated with three test cases in figure 6.

This finding tells us that the critical value χ_1^* can be obtained from the shape of the exotic cylinder without solving $L_0\varphi_0 = 0$. The property of the exotic cylinder is also closely related to the floating phenomenon. For the two-dimensional case, the analytical expression (3.21) for χ_1^* can be obtained from the relation between the variations δH and δU. A different point of view is provided when the exotic cylinder is regarded as a special floating body with a fixed position in which the contact point is allowed to move continuously on the solid. From this perspective, the formula (3.30) for calculating χ_1^* directly is proposed. Additionally, the formula (3.30) can also be applied to the determination of the maximal stable profile. Results show that the critical values χ_1^* calculated by solving $L_0\varphi_0 = 0$ and by (3.30) agree very well. These promising results may reveal new insights into stability analysis.

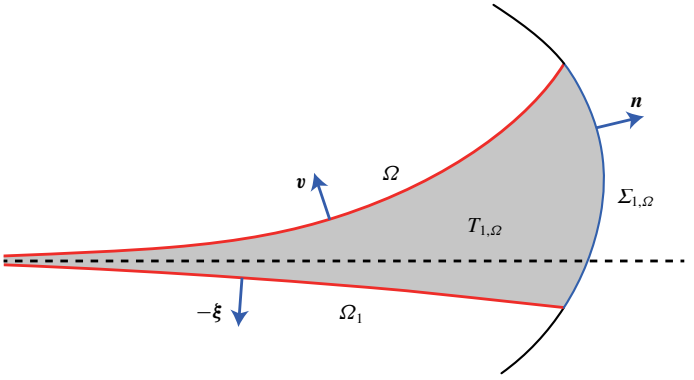

FIGURE 8. Comparison of Ω and Ω_1 for $K_{in} \leqslant 0$. Here $\Sigma_{1,\Omega}$ is the part of Σ between Ω and Ω_1, and $T_{1,\Omega}$ is the region bounded by Ω_1, $\Sigma_{1,\Omega}$ and Ω. The dashed line is the water line. Menisci Ω and Ω_1 are asymptotic to the water line at infinity. Vectors $\boldsymbol{v}$, $\boldsymbol{n}$ and $-\boldsymbol{\xi}$ are the outward unit normal vectors on Ω, $\Sigma_{1,\Omega}$ and Ω_1, respectively.

Acknowledgement

This research was supported in part by the National Natural Science Foundation of China (no. 11672116).

Appendix A

Wente (2011) has shown that any equilibrium meniscus is a minimiser of energy for the interior case $K_{in} > 0$. Following Wente (2011), we extend this result to the exterior and planar cases $K_{in} \leqslant 0$. Let Σ be an exotic cylinder with $K_{in} \leqslant 0$, $\{\Omega_t\}$ be a family of equilibrium menisci each of which meets Σ at a constant angle θ and T be the region bounded above by Ω, on the sides by Σ and below by a fixed equilibrium meniscus Ω_0. The potential energy (dimensionless) is given by (Wente 2011)

$$E(\Omega) = |\Omega| + \int_T U \mathrm{d}V - \cos\theta |\Sigma'|, \tag{A 1}$$

where Ω is an arbitrary admissible meniscus, $|\Omega|$ denotes the surface area of Ω and Σ' is the wetted part of Σ between Ω and Ω_0. We let $\boldsymbol{\xi} = \boldsymbol{\xi}(\boldsymbol{x})$ denote the upward-pointing unit normal vector field to $\{\Omega_t\}$. We have (see Wente 2011)

$$\nabla \cdot \boldsymbol{\xi} = -U \quad \text{in } T, \tag{A 2}$$

$$\boldsymbol{n} \cdot \boldsymbol{\xi} = -\cos\theta \quad \text{on } \Sigma. \tag{A 3}$$

By comparing the energies of an admissible meniscus Ω and an equilibrium meniscus Ω_1 (figure 8), we have

$$E(\Omega) - E(\Omega_1) = \lim_{R_b \to -\infty} (|\Omega| - |\Omega_1|) + \int_{T_{1,\Omega}} U \mathrm{d}V - \cos\theta |\Sigma_{1,\Omega}|, \tag{A 4}$$

where the left-hand points on the boundaries of Ω and Ω_1 are both located at $R_b \to -\infty$ because Ω and Ω_1 extend to infinity for $K_{in} \leqslant 0$. Applying the divergence theorem on the region $T_{1,\Omega}$ using the vector field $\boldsymbol{\xi}$, we find

$$-\int_{T_{1,\Omega}} U \mathrm{d}V = \int_{\Omega} (\boldsymbol{\xi} \cdot \boldsymbol{v} - 1)\, \mathrm{d}S + \lim_{R_b \to -\infty} (|\Omega| - |\Omega_1|) - \cos\theta |\Sigma_{1,\Omega}|. \tag{A 5}$$

Substituting (A 5) into (A 4), we obtain

$$E(\Omega) - E(\Omega_1) = \int_{\Omega} (1 - \boldsymbol{\xi} \cdot \boldsymbol{\nu}) \, \mathrm{d}S. \tag{A 6}$$

If $\Omega = \Omega_t$ is an equilibrium meniscus belonging to the family $\{\Omega_t\}$, then $E(\Omega_t) = E(\Omega_1)$. Furthermore, if Ω does not belong to $\{\Omega_t\}$, we have $E(\Omega) > E(\Omega_1)$. Thus, any equilibrium meniscus around the exotic cylinder with $K_{in} \leqslant 0$ is a minimiser of energy.

REFERENCES

ALEXANDER, J. I. D. & SLOBOZHANIN, L. A. 2004 A review of the stability of disconnected equilibrium capillary surfaces. *Microgravity Sci. Technol.* **15**, 3–21.

BHATNAGAR, R. & FINN, R. 2016 On the capillarity equation in two dimensions. *J. Math. Fluid Mech.* **18**, 731–738.

BOSTWICK, J. B. & STEEN, P. H. 2015 Stability of constrained capillary surfaces. *Annu. Rev. Fluid Mech.* **47**, 539–568.

CALLAHAN, M., CONCUS, P. & FINN, R. 1991 Energy minimizing capillary surfaces for exotic containers. In *Computing Optimal Geometries (with accompanying video tape)* (ed. J. E. Taylor), AMS Selected Lectures in Mathematics, pp. 13–15. American Mathematical Society.

CONCUS, P. 1968 Static menisci in a vertical right circular cylinder. *J. Fluid Mech.* **34**, 481–495.

CONCUS, P. & FINN, R. 1989 Instability of certain capillary surfaces. *Manuscr. Math.* **63**, 209–213.

CONCUS, P. & FINN, R. 1991 Exotic containers for capillary surfaces. *J. Fluid Mech.* **224**, 383–394.

CONCUS, P., FINN, R. & WEISLOGEL, M. 1992 Drop-tower experiments for capillary surfaces in an exotic container. *AIAA J.* **30**, 134–137.

CONCUS, P., FINN, R. & WEISLOGEL, M. 1999 Capillary surfaces in an exotic container: results from space experiments. *J. Fluid Mech.* **394**, 119–135.

DECKER, E. L., FRANK, B., SUO, Y. & GAROFF, S. 1999 Physics of contact angle measurement. *Colloids Surf.* A **156**, 177–189.

FINN, R. 1988 Non uniqueness and uniqueness of capillary surfaces. *Manuscr. Math.* **61**, 347–372.

FINN, R. 2010 On Young's paradox, and the attractions of immersed parallel plates. *Phys. Fluids* **22**, 017103.

GILLETTE, R. D. & DYSON, D. C. 1972 Stability of axisymmetric liquid-fluid interfaces towards general disturbances. *Chem. Engng J.* **3**, 196–199.

GULLIVER, R. & HILDEBRANDT, S. 1986 Boundary configurations spanning continua of minimal surfaces. *Manuscr. Math.* **54**, 323–347.

HILDEBRAND, R. E., HILDEBRAND, M. A. & TALLMADGE, J. A. 1971 Effect of radius on static menisci heights on wires. *Chem. Engng J.* **2**, 297–300.

HUH, C. & MASON, S. G. 1974 The flotation of axisymmetric particles at horizontal liquid interfaces. *J. Colloid Interface Sci.* **47**, 271–289.

HUH, C. & SCRIVEN, L. E. 1969 Shapes of axisymmetric fluid interfaces of unbounded extent. *J. Colloid Interface Sci.* **30**, 323–337.

KRAVCHENKO, V. V. & PORTER, R. M. 2010 Spectral parameter power series for Sturm–Liouville problems. *Math. Meth. Appl. Sci.* **33**, 459–468.

LOWRY, B. J. & STEEN, P. H. 1995 Capillary surfaces: stability from families of equilibria with application to the liquid bridge. *Proc. R. Soc. Lond.* A **449**, 411–439.

MADDOCKS, J. H. 1987 Stability and folds. *Arch. Rat. Mech. Anal.* **99**, 301–328.

MYSHKIS, A. D., BABSKII, V. G., KOPACHEVSKII, N. D., SLOBOZHANIN, L. A., TYUPTSOV, A. D. & WADHWA, R. S. 1987 Stability of equilibrium states of a liquid. In *Low-Gravity Fluid Mechanics*, pp. 120–218. Springer.

PERUZZO, P., DEFINA, A., NEPF, H. M. & STOCKER, R. 2013 Capillary interception of floating particles by surface-piercing vegetation. *Phys. Rev. Lett.* **111**, 164501.

PESCI, A. I., GOLDSTEIN, R. E., ALEXANDER, G. P. & MOFFATT, H. K. 2015 Instability of a Möbius strip minimal surface and a link with systolic geometry. *Phys. Rev. Lett.* **114**, 127801.

RAPACCHIETTA, A. V. & NEUMANN, A. W. 1977 Force and free-energy analyses of small particles at fluid interfaces: II. Spheres. *J. Colloid Interface Sci.* **59**, 555–567.

SLOBOZHANIN, L. A. & ALEXANDER, J. I. D. 2003 Stability diagrams for disconnected capillary surfaces. *Phys. Fluids* **15**, 3532–3545.

SLOBOZHANIN, L. A., ALEXANDER, J. I. D. & RESNICK, A. H. 1997 Bifurcation of the equilibrium states of a weightless liquid bridge. *Phys. Fluids* **9**, 1893–1905.

SLOBOZHANIN, L. A. & TYUPTSOV, A. D. 1974 Characteristic stability parameter of the axisymmetric equilibrium surface of a capillary liquid. *Fluid Dyn.* **9**, 563–571.

TYREE, M. T. 2003 Plant hydraulics: the ascent of water. *Nature* **423**, 923.

WENTE, H. C. 1999 Stability analysis for exotic containers. *Dyn. Contin. Discrete Impuls. Syst.* **5**, 151–158.

WENTE, H. C. 2011 Exotic capillary tubes. *J. Math. Fluid Mech.* **13**, 355–370.

WHITE, D. A. & TALLMADGE, J. A. 1965 Static menisci on the outside of cylinders. *J. Fluid Mech.* **23**, 325–335.

ZHANG, F., ZHOU, X. & ZHU, C. 2018 Effects of surface tension on a floating body in two dimensions. *J. Fluid Mech.* **847**, 489–519.